3

Fault diagnosis of electrical drives

Electrical drives are basic components in a multitude of devices, processes, machinery and vehicles, and in the large areas of mechanical power and process engineering, manufacturing, transportation and precision mechanical devices. Their power ranges from a few mW to hundreds MW.

The most important types of electrical motors can be divided into:

(i) DC motors
- series-wound motors
- shunt-wound motors
- permanent-field motors

(ii) Three-phase AC motors
- induction motors (asynchronous motors)
- synchronous motors

(iii) Single-phase AC motors
- commutator motors (universal motors)
- squirrel-cage motors.

Table 3.1 gives an overview of some basic types, illustrating torque characteristics and corresponding control inputs. As static and dynamic models of the various electrical motors are required for model-based fault detection, the reader is referred to well-known basic books on electrical drives such as [3.3], [3.13], [3.18], [3.19], [3.20].

In the following, some case studies are described for DC motors with brushes and for AC motors. Further types of electrical motors will be considered in Chapter 4 for electrical actuators.

3.1 Direct-current motor (DC)

3.1.1 Structure and models of a DC motor

A permanently excited DC motor with a rated power of $P = 550\,\mathrm{W}$ at rated speed $n = 2500\,\mathrm{rpm}$ is considered, [3.6]. This DC motor has a two-pair brush commuta-

R. Isermann, *Fault-Diagnosis Applications, Model-Based Condition Monitoring: Actuators, Drives, Machinery, Plants, Sensors, and Fault-tolerant Systems,*
DOI 10.1007/978-3-642-12767-0_3, © Springer-Verlag Berlin Heidelberg 2011

Table 3.1. General survey of electrical motors with small power, [3.9]

motor		DC shunt-wound motor	DC series-wound motor	three-phase asynchronous motor	three-phase synchronous motor (DC excitation of rotor)	single-phase (universal motor)	single-phase asynchronous motor with condensator	single-phase asynchronous motor (Ferraris motor)
circuit diagram		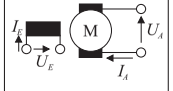	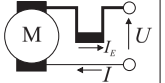	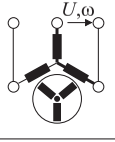	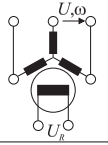	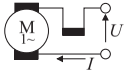	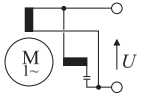	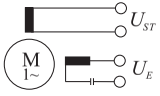
torque-speed characteristics		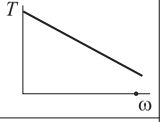	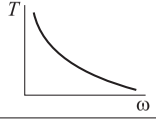	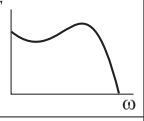	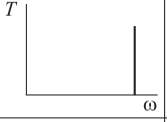	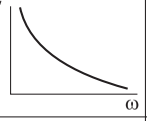	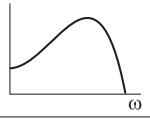	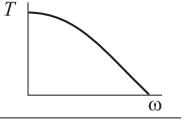
torque characteristics for manipulation	different manipul. variables:	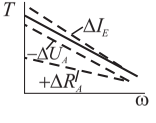	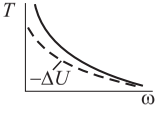	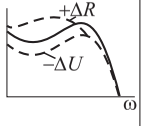	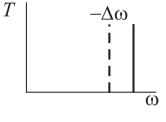	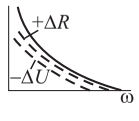		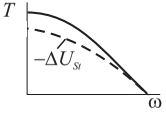
	normal:							
	manipulated variables	ΔU_A armature voltage ΔI_E excitation current ΔR_A armature resistance	ΔU voltage	ΔU voltage $\Delta\omega$ frequency ΔR rotor resistance	$\Delta\omega$ frequency	ΔU voltage ΔR armature resistance		ΔU_{St} manipulated voltage

tion, two pole pairs, and an analog tachometer for speed measurement; it operates against a hysteresis brake as load, see Figure 3.1. The measured signals are the armature voltage U_A, the armature current I_A and the speed ω. A servo amplifier with pulse-width-modulated armature voltage as output and speed and armature current as feedback allows a cascaded speed control system. The three measured signals first pass analog anti-aliasing filters and are processed by a digital signal processor (TXP 32 CP, 32-bit fpt, 50 MHz) and an Intel Pentium host PC. Also the hysteresis brake is controlled by a pulse-width servo amplifier. Usually such DC motors can be described by linear dynamic models.

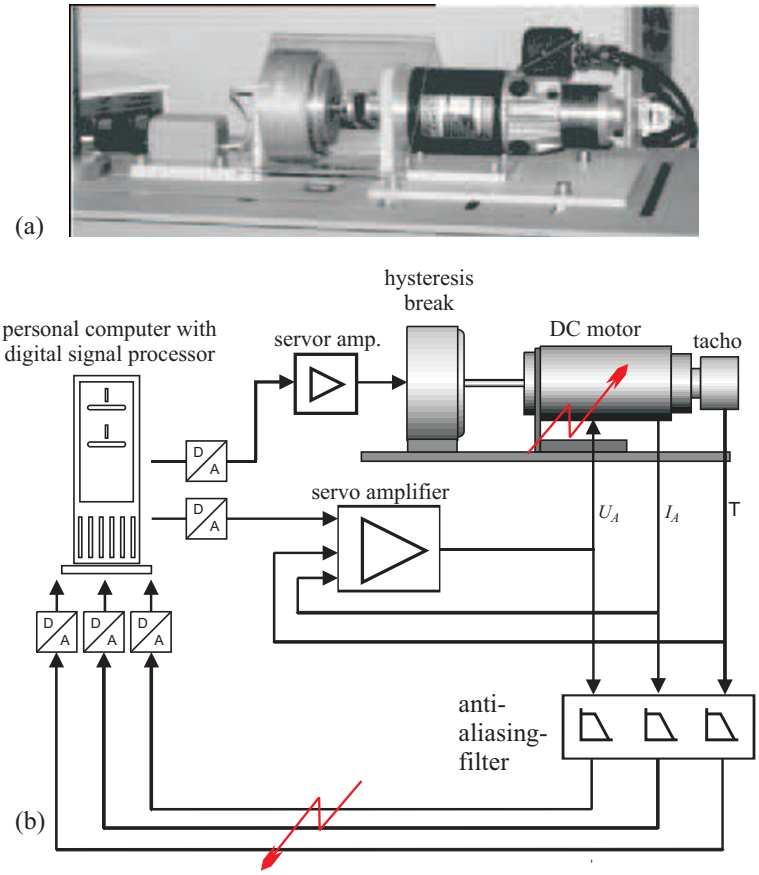

Fig. 3.1. DC motor test bench with hysteresis brake: a) test bench; b) scheme of equipment

However, experiments have shown that this model with constant parameters does not match the process in the whole operational range. Therefore, two nonlinearities are included so that the model fits the process better. The resulting first-order differential equations are:

$$L_A\ \dot{I}_A(t) = -R_A\ I_A(t) - \Psi\ \omega(t) - K_B|\omega(t)|\ I_A(t) + U_A^*(t) \tag{3.1.1}$$

$$J\ \dot{\omega} = \Psi\ I_A(t) - M_{F1}\ \omega(t) - M_{F0}\ \text{sign}\ (\omega(t)) - M_L(t) \tag{3.1.2}$$

Figure 3.2 depicts the resulting signal flow diagram. The term $K_B|\omega(t)|I_A(t)$ compensates for the voltage drop at the brushes in combination with a pulse-width-modulated power supply. The friction is included by a viscous- and a dry-friction term $M_{F1}\omega$ and $M_{F0}\text{sign}(\omega)$, see also [3.9]. The parameters are identified by least-squares estimation in the continuous-time domain, [3.6]. Table 3.2 gives the nominal values. Most of them ($R_A, \Psi, K_B, M_{F1}, M_{F0}$) influence the process gain, and the other two (L_A, J) the time constants. The signals U_A^*, I_A and ω are measured with a sampling frequency of 5 kHz, and state-variable filtered by a fourth-order low-pass filter with Butterworth characteristic and a cut-off frequency of 250 Hz.

Table 3.2. Data for the DC motor

armature resistance	$R_A = 1.52\ \Omega$
armature inductance	$L_A = 6.82 \cdot 10^{-3}\ \Omega\ \text{s}$
magnetic flux	$\Psi = 0.33\ \text{V s}$
voltage drop factor	$K_B = 2.21 \cdot 10^{-3}\ \text{V s / A}$
inertia constant	$J = 1.92 \cdot 10^{-3}\ \text{kg m}^2$
viscous friction	$M_{F1} = 0.36 \cdot 10^{-3}\ \text{Nm s}$
dry friction	$M_{F0} = 0.11\ \text{Nm}$

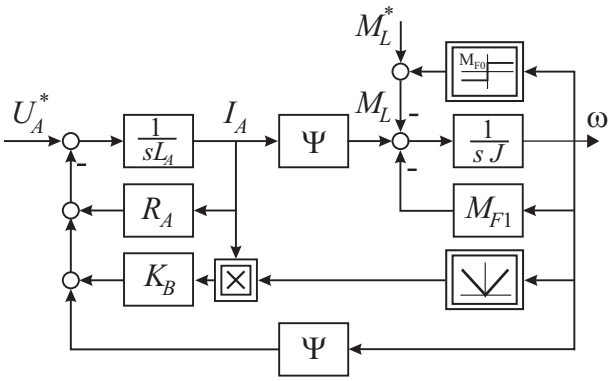

Fig. 3.2. Signal flow diagram of the considered DC motor

3.1.2 Fault detection with parity equations

For the detection and isolation of sensor (output) and actuator (input) faults a set of structured parity equations with state-space models according to Section 2.5 is applied.

As the differential equations (3.1.1) and (3.1.2) are nonlinear, the design procedure for a linear parity space cannot be applied directly. But defining $U_A^* - K_B|\omega(t)|I_A$ as voltage input U_A and as load input $M_L = M_{F0}\,\mathrm{sign}\,\omega$ leads to a linear description. The linear state-space representation then becomes

$$\begin{aligned}\dot{\mathbf{x}} &= \begin{bmatrix} \dot{I_A} \\ \dot{\omega} \end{bmatrix} = \begin{bmatrix} -\frac{R_A}{L_A} & -\frac{\Psi}{L_A} \\ \frac{\Psi}{J} & -\frac{M_F}{J} \end{bmatrix} \begin{bmatrix} I_A \\ \omega \end{bmatrix} + \begin{bmatrix} \frac{1}{L_A} & 0 \\ 0 & -\frac{1}{J} \end{bmatrix} \begin{bmatrix} U_A \\ M_L \end{bmatrix} \\ \mathbf{y} &= \begin{bmatrix} I_A \\ \omega \end{bmatrix} = \begin{bmatrix} 1 & 0 \\ 0 & 1 \end{bmatrix} \mathbf{x} \end{aligned} \tag{3.1.3}$$

A corresponding signal flow diagram is depicted in Figure 3.2.

An observability test reveals that both outputs (I_A and ω) can also observe each other. This is a precondition for a parity space of full order (here: 2). Then, $\mathbf{W}$, see Table 2.4 and [3.10] Equation (10.52), is chosen such that a set of *structured residuals* is obtained, where residual $r_1(t)$ is independent of $M_L(t)$, $r_2(t)$ of $U_A(t)$, $r_3(t)$ of $\omega(t)$ and $r_4(t)$ of $I_A(t)$, see also [3.6], [3.16], [3.4]:

$$\mathbf{W} = \begin{bmatrix} R_A & \Psi & L_A & 0 & 0 & 0 \\ -\Psi & M_{F1} & 0 & J & 0 & \\ \alpha & 0 & \beta & 0 & JL_A & 0 \\ 0 & \alpha & 0 & \beta & o & JL_A \end{bmatrix} \tag{3.1.4}$$

with $\alpha = \Psi^2 + R_A\, M_{F1}$;
$\beta = L_A\, M_{F1} + J\, R_A$.
The residuals, using three measured signals, then follow as:

$$\begin{aligned} r_1(t) &= L_A\, \dot{I}_A(t) + R_A\, I_A(t) + \Psi\, \omega(t) - U_A(t) \\ r_2(t) &= J\, \dot{\omega}(t) - \Psi\, I_A(t) + M_{F1}\, \omega(t) + M_L(t) \\ r_3(t) &= J\, L_A\, \ddot{I}_A(t) + (L_A\, M_{F1} + J\, R_A)\, \dot{I}_A(t) \\ &\quad + (\Psi^2 + R_A M_{F1}) I_A(t) - J\, \dot{U}_A(t) - M_{F1}\, U_A(t) - \Psi\, M_L(t) \\ r_4(t) &= J\, L_A\, \dddot{\omega}(t) + (L_A\, M_{F1} + J\, R_A)\, \ddot{\omega}(t) + (\Psi^2 + R_A\, M_{F1})\, \omega(t) \\ &\quad - \Psi\, U_A(t) + L_A\, \dot{M}_L(t) + R_A\, M_L(t) \end{aligned} \tag{3.1.5}$$

The same residual equations can be also obtained via transfer functions as described in Example 10.3 in [3.10]. If an additive fault of the measured signals and of M_L occurs, all residuals except the decoupled one are deflected. The scheme of the structured residuals is not touched by the compensation for the nonlinear voltage drop of the brushes, as its magnitude is small enough. Two parameters R_A and M_{F1}, however, depend on the present motor temperature. The behavior of R_A and its effect on residual r_1 is depicted in Figure 3.3. Therefore, the use of adaptive parity equations improves the residual performance, see [3.6] and [3.10].

The residuals are now examined with regard to their sensitivity to additive and parametric faults. As r_1 and r_2 comprise all parameters and all signals, it is sufficient to consider only these two, although r_3 or r_4 can also be taken. From (3.1.5) it yields

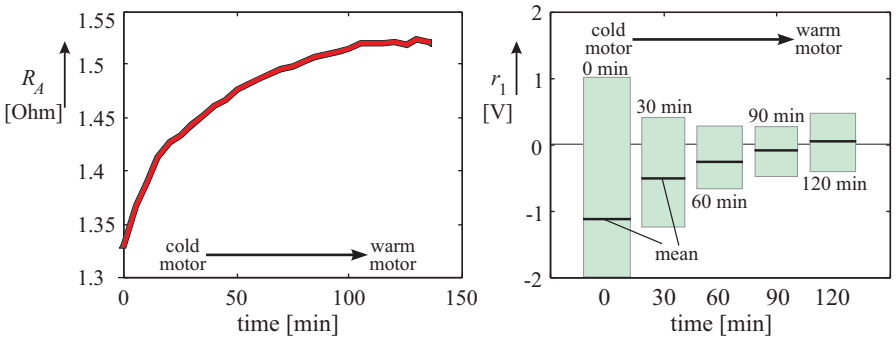

Fig. 3.3. Influence of the motor temperature on resistance R_A and residual r_1

$$\begin{aligned} r_1(t) &= \Delta\, L_A\, \dot{I}_A(t) + \Delta\, R_A\, I_A(t) + \Delta\, \Psi\, \omega(t) \\ &\quad + L_A\, \Delta\, \dot{I}_A(t) + R_A\, \Delta\, I_A(t) + \Psi\, \Delta\, \omega(t) - \Delta\, U_A(t) \\ r_2(t) &= +\Delta\, J\, \dot{\omega}(t) - \Delta\, \Psi\, I_A(t) + \Delta\, M_{F1}\, \omega(t) \\ &\quad + J\, \Delta\, \dot{\omega}(t) - \Psi\, \Delta\, I_A(t) + M_{F1}\, \Delta\, \omega(t) + \Delta\, M_L(t) \end{aligned} \tag{3.1.6}$$

In the presence of residual noise, e.g. of r_1 with a magnitude of about 1 V and an armature current of 3 A, a resistance change must be at least 0.3 Ω in order to deflect the residual significantly. Therefore, the two linear parameters R_A and M_{F1} are selected to be tracked according to a single parameter estimation together with parity equations, as described in [3.10], Section 10.5. The forgetting factor is chosen as $\lambda = 0.99$.

3.1.3 Fault detection with parameter estimation

The parameter estimation is based on the two differential equations (3.1.1) and (3.1.2) in the simplified form

$$\dot{I}_A(t) = -\hat{\theta}_1\, I_A(t) - \hat{\theta}_2\, \omega(t) + \hat{\theta}_3\, U_A(t) \tag{3.1.7}$$

$$\dot{\omega}(t) = \hat{\theta}_4\, I_A(t) - \hat{\theta}_5\, \omega(t) - \hat{\theta}_6\, M_L(t) \tag{3.1.8}$$

with the process coefficients

$$R_A = \frac{\hat{\theta}_1}{\hat{\theta}_3};\; L_A = \frac{1}{\hat{\theta}_3};\; \Psi = \frac{\hat{\theta}_2}{\hat{\theta}_3} \text{ and } \Psi = \frac{\hat{\theta}_4}{\hat{\theta}_6};\; J = \frac{1}{\hat{\theta}_6};\; M_{F1} = \frac{\hat{\theta}_5}{\hat{\theta}_6} \tag{3.1.9}$$

Applying the recursive parameter estimation method DSFI (discrete square-root filtering in information form), [3.11], with forgetting factor $\lambda = 0.99$ yields the parameters $\hat{\theta}_i$ by using three measured signals. Then all process coefficients can be calculated with (3.1.9). Experimental results with idle running ($M_L = 0$) resulted in standard deviations of the process coefficients in the range of $2\% < \sigma_\theta < 6.5\%$, [3.6].

3.1.4 Experimental results for fault detection (SELECT)

Based on many test runs, five different faults are now selected to show the detection of additive and multiplicative faults with parity equations and recursive parameter estimation, [3.5]. The time histories depict the arising faults at $t = 0.5\,\mathrm{s}$. The faults are step changes and were artificially produced. Figure 3.4 shows the parameter estimates and the residuals of parity equations. The residuals are normalized by division through their thresholds. Therefore, exceeding of 1 or -1 indicates the detection of a fault. In the cases a) to d) and f) the DC motor is excited by a pseudo random binary signal (PRBS) of the armature voltage U_A which is a requirement for dynamic parameter estimation, as shown in Figure 3.4f). In case e) the input is constant. The results can be summarized as:

a) A sensor-gain fault of the voltage sensor U_A leads as expected to a change of residual 1 (and 3, 4) but not of residual 2, which is independent of U_A. The parameter estimates show (incorrect) changes for R_A, L_A and Ψ, because the gain of the voltage sensor is not modeled
b) An offset fault in the speed sensor ω leads to a change of the residuals r_4, r_1 and r_2, but r_3 remains uneffected, because it is independent of ω. The parameter estimate of Ψ shows an (incorrect) change
c) A multiplicative change of the armature resistance R_A yields a corresponding change of the parameter estimate $\hat{R}_A$. However, the residuals increase their variance drastically and exceed their thresholds
d) A change of the ratio of inertia is correctly given by the parameter estimate $\hat{J}$. But all residuals, except r_1, exceed their thresholds by increasing their variance
e) The same fault in R_A as in c) is introduced, but the input U_A is kept constant. The parameter estimate $\hat{R}_A$ does not converge to a constant value and the parity equation residuals r_1 and r_4 change their mean, however, with large variance
f) A brush fault leads to an increase of R_A and L_A but not of Ψ. The residuals show an increase of the variance.

Table 3.3 summarizes the effects of some investigated faults on the parameter estimates and parity residuals.

These investigations have shown:

1) *Additive faults* like the offsets of sensors are well detected by the parity equations. They react fast and do not need an input excitation for a part of the faults. However, they have a relatively large variance, especially if the model parameters do not fit well to the process
2) *Multiplicative faults* are well detected by parameter estimation, also for small faults. Because of the inherent regression method the reactions are slower but smoothed. But they require an input excitation for dynamic process models.

Therefore, it is recommended to combine both methods, as shown in [3.10], Section 14.3. The parity equations are used to detect changes somewhere in the process and if the fault detection result is unclear a parameter estimation is started, eventually by a dynamic test signal for some seconds. If the motor operates dynamically

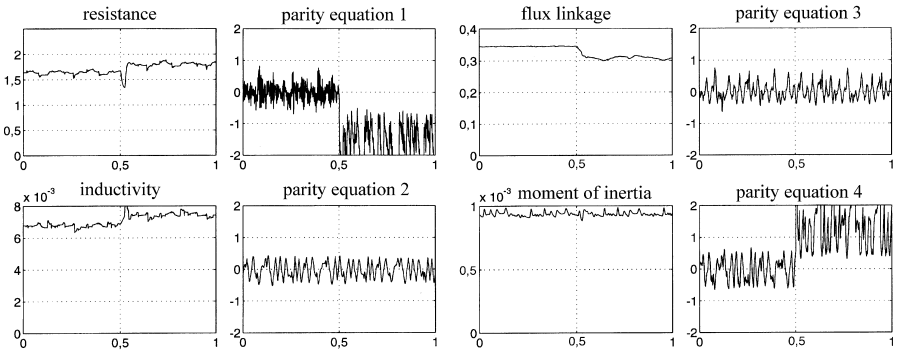

(a) sensor-gain fault (ΔU_A : +10%)

(b) DC value sensor fault ($\Delta\omega$: 10%)

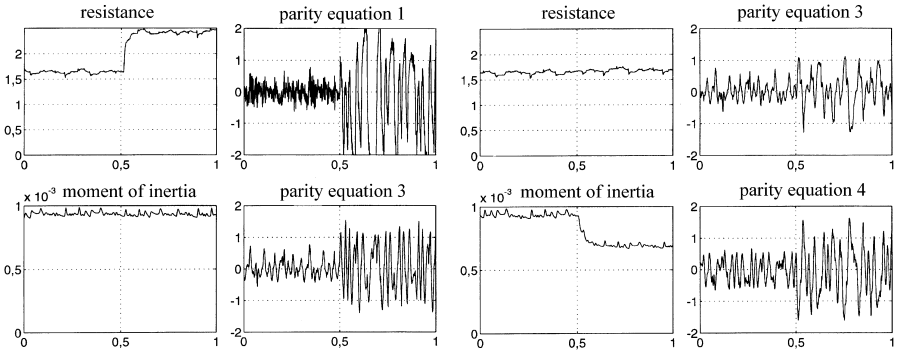

(c) change of armature resistance (ΔR_A: +50%)

(d) change of moment of interia (ΔJ: -30%)

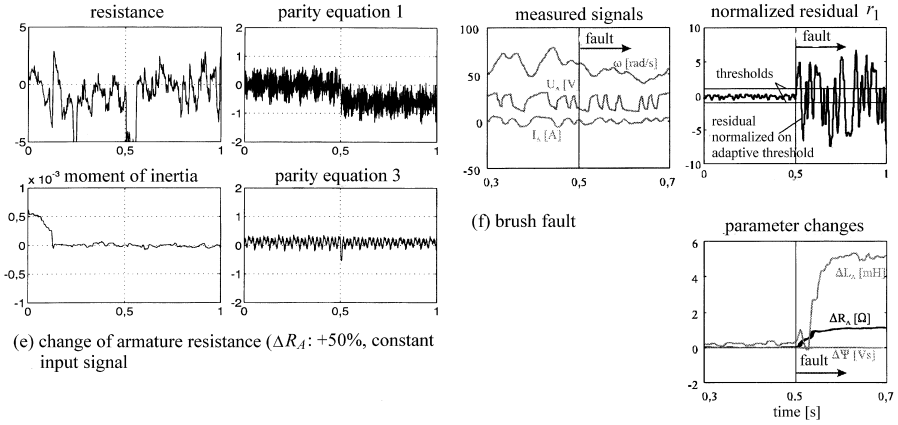

(e) change of armature resistance (ΔR_A: +50%, constant input signal

(f) brush fault

Fig. 3.4. Time histories of signals, residuals of parity equations and parameter estimation at fault occurrence

- parameter estimates: R_A resistance, L_A inductivity, Ψ flux linkage, J_A moment of inertia
- parity equations: r_1, r_2, r_3, r_4

Table 3.3. Fault-symptom table for the fault detection of a DC motor with dynamic input excitation $U_A(t)$ in the form of a PRBS. + positive deflection; ++ strong positive deflection; 0 no deflection; − negative deflection; − − strong negative deflection; ± increased variance

faults			symptoms								
			parameter estimation					parity equations			
			R_A	L_A	Ψ	J	M_{F1}	r_1	r_2	r_3	r_4
parametric faults	armature resistance	ΔR_A	++	0	0	0	0	±	0	±	±
	brush fault		++	+	0	0	0	±	0	±	±
	change of inertia	ΔJ	0	0	0	++	0	0	±	±	±
	change of friction	ΔM_{F1}	0	0	0	0	++	0	±	±	±
	voltage sensor gain fault	ΔU_A	±	±	±	0	0	−	0	−	−
additive faults	speed sensor offset fault	$\Delta\omega$	0	0	−	0	0	+	+	0	+
	current sensor offset fault	ΔI	±	±	±	0	0	+	−	+	0

anyhow (as for servo systems and actuators) then the parameter estimation can be applied continuously, but with a supervision scheme, see [3.11].

[3.6] has shown that a considerable improvement can be obtained by continuously estimating the armature resistance with a single parameter estimation using parity equations in order to reach the temperature dependent resistance parameters, [3.7]. Furthermore, adaptive thresholds are recommended, to compensate for model uncertainties, see Section 2.4.4.

3.1.5 Experimental results for fault diagnosis with a learning fault-symptom tree

The model-based fault-detection system with parity equations and parameter estimation is now the basis for a fault-diagnosis procedure. As described in Section 2.6 the method for fault diagnosis can be divided in classification and inferencing. A first simple classification is the use of fault-symptom tables and pattern recognition as in Table 3.3. Also decision trees belong to the class of classification methods. However, a combination with a neuro-fuzzy structure gives them a learning behavior of fuzzy if-then rules with AND operators, forming an adaptive inference method, called SELECT, [3.4]. This is applied in the following to the DC motor test bench.

a) The symptoms used

To diagnose the faults, altogether 22 symptoms are created:

- Windowed sums of the absolute values of the three measured signals U_A^*, I_A, ω
- Mean values and standard deviations of four residuals: $\bar{r}_1, \ldots, \bar{r}_4$ and $\bar{\sigma}_{r1}, \ldots, \bar{\sigma}_{r4}$

- Eight parameter estimates. Symptoms are the deviations of the current values – results of the estimation – from the nominal ones. They are normalized to the nominal values. For the rotor resistance R_A this is $\Delta R_{A1} = \frac{(R_{A,nom.} - R_{A,est.})}{R_{A,nom.}}$. The index 1 denotes that the estimation was carried out using the first parity equation. Similarly, ΔR_{A4}, ΔL_{A1}, ΔL_{A4}, ΔJ_2, ΔJ_3, ΔM_{F12}, and ΔM_{F13} are computed
- Additionally, two symptoms judge the quality of the estimation. They describe the variance of an estimated parameter during a recursive estimation. This variance can give a good indication whether the structure of the estimation equation is valid. A structural change of the system will result in a bad estimation result where the recursively estimated parameters fluctuate significantly. Two parameter estimations were chosen: Ψ and M_{F1}. Their estimation variances are denoted by $\sigma_{est.,\Psi}$ and $\sigma_{est.,MF1}$.

The symptoms serve to differentiate between 14 fault situations that can artificially be introduced on the test rig.

The DC motor diagnosis was performed by learning a SELECT tree from experimentally gained fault data. For the fault cases, typically 10–50 test-cycle measurements for a parameter estimation were performed. The residuals were computed from the test runs. That way, each test run results in one data point in the symptom space. The membership functions were created with the degressive fuzzy-c-means method. To utilize a maximum of transparency and create a highly interpretable system, prior knowledge was used to structure the diagnosis system.

b) Incorporation of structural knowledge

In most applications, a certain amount of knowledge about the symptom behavior is present. Even if exact values for thresholds etc. are not known, there usually is some insight into the process like physical understanding of similar faults or similar effects of faults on certain symptoms. For the DC motor, this could be as simple as to use the windowed sums of the signals in order to to detect a broken sensor cable. This information is quite obvious, but its benefits are sometimes neglected, if a diagnosis system is designed with the aim to be solely learned from measured data. Hence, the task could be simpler if the designer used this information from the beginning.

Furthermore, the selection of the symptoms for the diagnosis becomes a matter of *robustness*. Some symptoms are affected by faults for which they are not an appropriate indicator. In an experimental environment, it is virtually impossible to gather enough measurements to adequately reflect every influence. Especially changes in the environmental conditions and long-term changes due to wear are hardly captured in a limited time frame. This leads to diagnosis systems that work well under the experimental conditions but fail otherwise. The diagnosis of a fault should therefore be based on the *appropriate subset* of all available symptoms. Only the relevant ones should be selected.

Often, different faults can be categorized into larger groups if their effects on the process are similar. It is then advantageous to find a classification system for

the larger groups first and later separate within them. This leads to the concept of a *hierarchical* diagnosis system.

Overall, it is proposed to use prior knowledge to *structure* the diagnosis system. The designer builds groups of faults and identifies the corresponding relevant symptoms to first differentiate between and later within them. The exact decisions can be found automatically if enough measured data is available.

If the set of all different fault situations F_i is denoted by

$$\mathcal{F} = \{F_1, F_2, \ldots F_r\} \tag{3.1.10}$$

and the available symptoms given by

$$\mathcal{S} = \{s_1, s_2, \ldots s_t\} \tag{3.1.11}$$

one can form meta-classes $\mathcal{C}_i, i = 1 \ldots m$ with

$$\mathcal{F} = \mathcal{C}_1 \cup \mathcal{C}_2 \cup \ldots \cup \mathcal{C}_m \tag{3.1.12}$$

In the DC motor diagnosis, for instance, such a meta-class is given by all faults on the mechanics of the motor. Such a hierarchy based on meta-classes requires at least $q = m + r$ decisions d_j, $j = 1 \ldots q$ assumed that no $\mathcal{C}_i$ is a single-element set. Each d_j is based on a subset $\mathcal{S}_{dj} \in \mathcal{S}$. The SELECT approach will then produce a system with p parameters where p is given by

$$p = \sum_{j=1}^{q} \text{card}\,(\mathcal{S}_{dj}) \tag{3.1.13}$$

which is typically much less than a parallel network structure would result in (cardinalities are the number of relevant sets). The usually larger number of parameters in parallel network configurations can lead to slower convergence and ill-conditioned optimization problems.

In addition to the structural knowledge, one can incorporate more detailed knowledge into the individual rules if desired.

c) Results with SELECT method

A total of 14 different fault situations are applied on the DC motor test bench:

- Change of rotor inductance or resistance F_{RA}, F_{LA}
- Broken rotor wiring (F_W)
- Failure of one the four brushes (F_B)
- Increased friction in the bearings (F_F)
- Offset on voltage, current or speed sensor signal ($F_{O,UA}$, $F_{O,IA}$, $F_{O,\omega}$)
- Gain change of voltage, current or speed sensor signal ($F_{G,UA}$, $F_{G,IA}$, $F_{G,\omega}$)
- Complete voltage, current or speed sensor failure (F_{UA}, F_{IA}, F_{ω}).

Repeated experiments with different faults were performed using a test cycle. The symptoms described in a) were computed for each of the experiments. Overall, the training set for the approach consisted of data from 140 experiments.

Figure 3.5 shows the resulting structure for the DC motor diagnosis. Details have been omitted to visualize the concept only. Each block comprises a meta-class $\mathcal{C}_1$ of faults. Every branching of the tree is connected to a decision d_j learned with the SELECT approach, i.e. it contains a fuzzy rule. In each meta-class, a classification tree decides which individual fault has occurred based on a subset $\mathcal{S}_i$ of the symptoms.

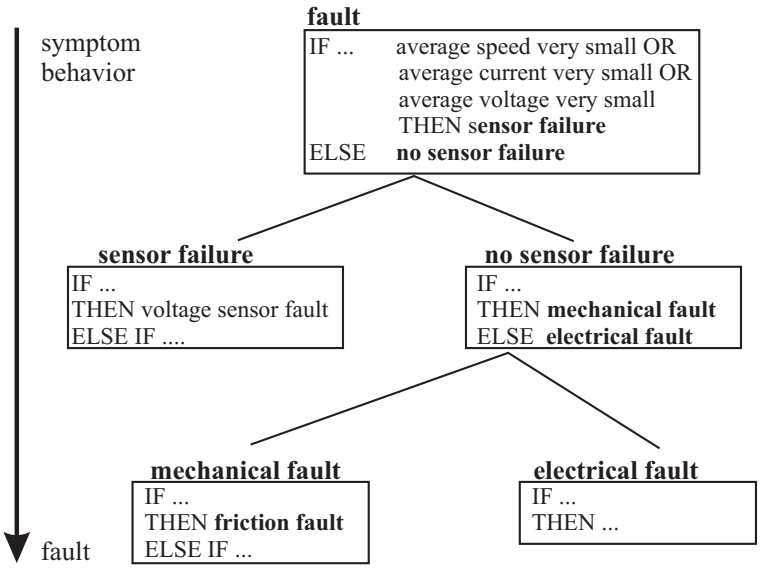

Fig. 3.5. Hierarchical fault-diagnosis system. Each block comprises a fuzzy classification tree

The hierarchical decision tree proved to be highly suitable for the diagnosis. It achieved a 98% classification rate in a cross-validation scheme.

The groups of faults have been selected following basic understanding of the DC motor supervision concept. Firstly, the three total sensor breakdowns are different from other faults due to their strong effects on all symptoms. They form the first meta-class $\mathcal{C}_1$ and can be easily differentiated by the three windowed sums of the signals. These three symptoms accordingly form the set $\mathcal{S}_1$.

Since the motor can be understood as a combination of an electrical and a mechanical component, faults on these two parts were again treated separately, creating two more meta-classes, $\mathcal{C}_2$ and $\mathcal{C}_3$. Accordingly, the appropriate subsets of symptoms $\mathcal{S}_2$ and $\mathcal{S}_3$ for the diagnosis were selected. Basically, $\mathcal{S}_2$ and $\mathcal{S}_3$ consist of the residuals and parameter deviations connected to the corresponding meta-class. The diagnosis of electrical faults, for instance, is not based on parameter estimates of the mechanical parameters. Although some electrical faults may have an influence on the estimates of the mechanical parameters, this influence should not be

used as the estimates are misleading and not reliable. Hence, $\mathcal{S}_2$ does not contain $\Delta J_2, \Delta J_3, \Delta M_{F12}$ or ΔM_{F13}.

To give an example of the SELECT approach, the rules for the distinction of the electrical faults are given below:

$$\begin{aligned}
&\text{IF } \bar{r}_1 \text{ is small AND } \Delta L_{A4} \text{ is strongly negative THEN Fault } F_{LA}\\
&\text{ELSE IF } \bar{r}_1 \text{ is small AND } \bar{\sigma}_{r4} \text{ is medium THEN Fault } F_{RA}\\
&\text{ELSE IF } \bar{r}_1 \text{ is small AND } \bar{\sigma}_{r4} \text{ is large THEN Fault } F_B\\
&\text{ELSE IF } \bar{r}_2 \text{ is not small THEN Fault } F_{0,IA}\\
&\text{ELSE IF } \bar{r}_1 \text{ is small THEN Fault } F_{G,IA}\\
&\text{ELSE IF } \bar{r}_1 \text{ is large AND } \sigma_{est.,\Psi} \text{ is not small THEN Fault } F_{0,UA}\\
&\text{ELSE Fault } F_{G,UA}
\end{aligned} \tag{3.1.14}$$

The relevance indices of the rule premises are not listed here. They also play a role for the exact decision boundaries.

Nevertheless, it is possible to analyze and understand parts of these rules. Clearly, the rules reveal the discriminatory power of the first residual, since it was used very often. Other rule premises are also understandable. The change of the rotor inductance is indicated by a strongly negative estimation of this change magnitude. Compare this rule to Figure 3.6a). It shows the values ΔL_{A4} for the electrical faults from the training set. Clearly, the fault F_{LA} makes a distinct difference. Hence, it makes sense to use ΔL_{A4} to distinguish the fault from the others. The corresponding membership functions are shown in Figure 3.6b). It must be noted that the experimental setup allowed only a fixed deviation of the inductance by –50% as a fault. That can be seen in the estimation result. If, however, also positive changes are to be diagnosed, one is able to enhance the rule manually. For instance, one could use

$$\text{IF } \bar{r}_1 \text{ is small AND } \Delta L_{A4} \text{ is not small THEN Fault } F_{LA} \tag{3.1.15}$$

The corresponding membership functions for ΔL_{A4} would also have to be adapted accordingly to allow processing of positive values of ΔL_{A4}.

Another interesting observation is the use of $\sigma_{est.,\Psi}$ in the sixth rule of (3.1.14) to distinguish offset from gain faults of the voltage sensor. This can be explained by the fact that an offset term in the estimation equation given by an offset fault will change the *structure* of the estimation equation, while a gain will only effect parameters. Hence, the normal estimation equation will still be valid in the case of gain faults, but indicate a problem by a large $\sigma_{est.,\Psi}$ for offset faults.

The system performed well on new experiments, showing the increased robustness through the incorporation of very simple knowledge. Additionally, the system has a higher degree of transparency facilitating an adaptation to other motors. The diagnostic rules can be extracted and are largely understandable.

d) Relation to fault trees

The resulting hierarchical classifier can also be interpreted as a set of fuzzy fault trees. If one *reverses* the order of the structure and traces the decisions leading to a

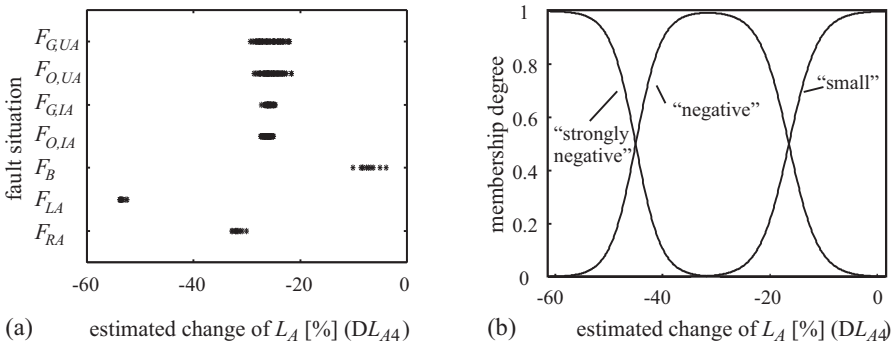

Fig. 3.6. Estimated rotor inductance computed from the fourth parity residual. Apparently, most faults influence the result, however, the faulty inductance can most easily be detected due to its strong influence: a) estimation results; b) resulting membership functions

particular fault back through the tree, it is possible to explicitly draw a fault tree for each individual fault. Figure 3.7 shows one fault situation (increased friction in the motor) as an example. The intermediate steps like "mechanical fault" from Figure 3.7 become *events* of the fault tree.

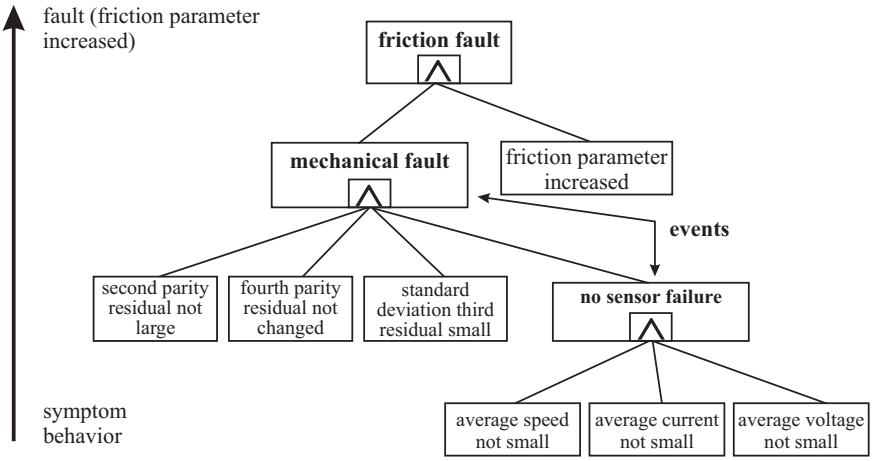

Fig. 3.7. Fault tree for one particular fault extracted from the diagnostic tree in Figure 3.5

Similar fault trees can be constructed for the other faults. This requires one to analyze the rule tree and explicitly draw the trees. The resulting set of trees is a relatively redundant representation of the fault-symptom relation because the same events are used in multiple trees. They are nevertheless very intuitive and serve to understand and visualize the functionality of the diagnostic system.

e) Computational demands

The most time-critical computation of the presented supervision concept is the computation of the continuous-time residuals. They require the evaluation of state-variable filters that are difficult to implement in fixed-point arithmetic. If the computational resources are limited, also a discrete-time form of the residuals is possible. This has, for instance, been implemented by [3.17].

The diagnosis, on the other hand, only needs to be evaluated if the fault-detection thresholds are violated. It is not time critical and can, for instance, be computed as a background job in the motor controller. Similarly, floating-point computations such as for the computation of the exponential function in the SELECT neuron can always be implemented on a lower-precision fixed-point controller, for instance, by using lookup tables. If the computational time is not critical, one can also implement floating-point arithmetic on fixed-point controllers. Since the time needed for the diagnosis is small compared with the time that typically is needed for personnel to reach a faulty device, it is obvious that the computational demand should not really be an issue. Safety-critical measures can be taken as soon as the thresholds are violated even before the diagnosis is started.

3.1.6 Conclusions

The detailed theoretical and experimental investigations with the permanently excited DC motor in idle running or with load have demonstrated that it is possible to detect 14 different faults by measurement of only three signals and combination of the parity equation and parameter estimation approach. Additive faults, like offsets of sensors, are easily detectable by parity equations in normal operation without extra input excitation signals. Multiplicative faults, like parameter deviations of the motor are better detected by parameter estimation, but require appropriate input excitation signals, at least for short times. The described methods can be transformed to other types of DC motors, depending on their construction, and also to single-phase AC motors. Further, by applying the self-learning neuro-fuzzy system SELECT all faults could be diagnosed with a 98% correct classification rate. A selection of faults, especially in the mechanical parts can also be detected by applying only signal models for current structure-borne vibrations, [3.2].

3.2 Alternating-current motor (AC)

Alternating-current motors in the form of induction or asynchronous motors consist usually of three windings placed in stator slots that are interconnected with the individual phases of a three-phase voltage supply system either in delta- or Y-connection, see Figure 3.8a). A rotating magnetic field is generated where angular velocity depends on the power supply frequency f and on the number of pole pairs p within the stator. Depending on different rotor constructions, induction motors and synchronous motors can be distinguished. In the following, induction motors with a squirrel-cage

http://www.springer.com/978-3-642-12766-3

Fault-Diagnosis Applications
Model-Based Condition Monitoring: Actuators, Drives, Machinery, Plants, Sensors, and Fault-tolerant Systems
Isermann, R.
2011, XVI, 354 p., Hardcover
ISBN: 978-3-642-12766-3